46th AIAA Aerospace Sciences Meeting and Exhibit
7 - 10 January 2008, Reno, Nevada

AIAA 2008-911

The Optimum Vacuum Nozzle: an MDO Approach

Colonno, M. R.[1]
Stanford University, Palo Alto, California, 94305 and
Space Exploration Technologies, Hawthorne, CA, 90250

Van der Weide, E.[2]
Stanford University, Palo Alto, California, 94305

and

Alonso, J. J .[3]
Stanford University, Palo Alto, California, 94305

A multidisciplinary optimization (MDO) methodology for the design of vacuum nozzles is presented, based on the maximization of the total stage or vehicle velocity increment. Traditional design methodologies for vacuum nozzles are discussed and compared to an MDO-based approach which accounts for the size and mass of the nozzle as well as multidisciplinary performance trades. Various levels of analytical fidelity are discussed with respect to physical accuracy and computational cost. The method is tested in an example of CH_4-LOX nozzle and the results compared to the results of a traditional method. Finally, future directions and the use of higher-fidelity analytical tools are discussed.

Nomenclature

A	=	area
c	=	generic constraint function
C_F	=	thrust coefficient
c_p	=	specific heat at constant pressure
c_v	=	specific heat at constant volume
d	=	skin thickness
F	=	thrust
g_0	=	standard Earth gravity
I_{sp}	=	specific impulse
J	=	objective function
L	=	length
M	=	Mach number
m	=	mass
MS	=	margin of safety
N	=	number of cells
$\boldsymbol{n}$	=	outward unit normal vector
p	=	pressure
r	=	radial direction
$\boldsymbol{r}$	=	position vector
s	=	arc length
R	=	radius
$\Re$	=	gas constant
T	=	temperature
V	=	velocity

[1] Chief Aerodynamic Engineer, Space Exploration Technologies, Member AIAA
[2] Research Associate, Aeronautics & Astronautics, Stanford University, Member AIAA
[3] Associate Professor, Aeronautics & Astronautics, Stanford University, Member AIAA

x = axial direction
$\boldsymbol{x}$ = vector of design variables or unit axial vector
ε = tolerance
γ = ratio of specific heats c_p/c_v
ξ,η = mesh topology
ϕ = meridian angle
ρ = density
σ = stress

Subscripts

c = chamber quantity
e = exit plane or surface
h = hoop
m = meridian
min = minimum
max = maximum
NZ = nozzle
P = propellant
PL = payload
r = radial direction
S = structural
t = stagnation quantity
u = ultimate
w = evaluated at the wall
x = axial direction
y = yield
θ = circumferential direction

Superscripts

T = transpose
$*$ = optimum value or throat condition

I. Introduction

WHEN designing a vacuum nozzle, key trades exist in deciding upon the physical dimensions. A larger area ratio will produce a higher exit velocity and higher I_{sp}, but increase the inert mass of the vehicle or stage. In addition, when three-dimensional flow effects are included, a rapidly-diverging nozzle (larger R/L) will have higher three dimensional flow losses than a more gradually-diverging nozzle (smaller R/L) but also have lower mass. The local curvature and pressure profile of the nozzle will determine the stresses in the walls and hence the material thickness. Internal and external heat transfer is also a critical factor in nozzle design from both a structural and performance standpoint. The coupling of the internal flow properties to the propulsive performance, heat transfer, and wall stresses suggests a multidisciplinary approach to nozzle optimization.

Traditionally, rocket nozzles have been design exclusively for propulsive performance. The optimization of nozzles profiles for maximum thrust was pursued long before computational fluid mechanics (CFD) or multidisciplinary optimization (MDO) became widely-available tools. A numerical procedure, known as the *Rao Method*[8], involves stepping along flow characteristics which reflect off the nozzle walls from the throat to the exit plane. This procedure could be pursued by hand or with minimal computing power and repeated for various nozzle contours until a reasonable optimum was found. Though simple in formulation, this procedure yields remarkably valuable results and is still widely used in the preliminary design of rocket nozzles. Current computing power allows this method to be evaluated with essentially negligible computational cost and a large number of designs can be evaluated rapidly. Many modification and improvements have been studied since the original method was developed[1,5,9,18]. This approach, however, reflects the assumption that higher propulsive performance always yields

better vehicle or stage performance. When the mass of the entire system and the multidisciplinary trades are taken into account, this is not always the case. (This is analogous to comparing the aerodynamic and aero-structural optimum wing lift distributions.) Here we pursue a robust, optimizer-independent MDO architecture for the design of a general vacuum rocket nozzle for maximum system-level performance with manageable computational cost.

II. Problem Formulation

A relatively simple but representative nozzle profile was chosen consisting of a circular arc tangent to the horizontal at the throat and a parabola tangent to the circular arc, shown in Fig. (1). Given manufacturing constraints, each section was assumed to have a constant thickness. (It should be noted that tapering the thickness can be done practically; the constant thickness assumption was used here to simplify the problem dimensionality.) The throat radius, R^*, and combustion chamber conditions were fixed and the total length, L, exit radius, R_e, axial coordinate of the transition, x_{tr}, and thicknesses of each section, d_1 and d_2, were chosen as design variables. The stage (or vehicle) dry mass, m_S (not including the mass of the nozzle), and propellant mass, m_P, are system-level parameters. This simplified design thus contained five continuous design variables, shown in Eq. (1), and two scalar parameters. A generalized version of the design problem could contain a single continuous spline profile through N control points, yielding $2N$ variables (x_i,r_i) to specify the shape in addition to N thickness values, d_i. This is suggested as a higher-fidelity extension of this work but does not change the fundamental process discussed here.

Several simple geometric constraints were used to ensure a valid geometry and CFD mesh. *Geometric* constraints are emphasized as those evaluated analytically which not require a response surface. It was assumed the nozzle had to fit inside an interstage or some other primary structure before use, with global bounds on L and R_e stated in Eq. (2). The global bounds on x_{tr} simply mirrored those of L. The working units were meters for L, R_e, and x_{tr} and millimeters for the material thicknesses d_1 and d_2. The material thicknesses where constrained to minimum and maximum values practical for manufacturing. The cone angle, defined as the angle formed between a line connecting the edge of the throat to the edge of the exit, was constrained between β_{min} and β_{max} to avoid very narrow or very rapidly-diverging designs known a priori to be impractical in Eqs. (3). (This is essentially the same as constraining the L/R ratio of the nozzle.) An arbitrary lower limit of the profile dimensions, ε, was used to avoid problematic zero-length dimensions in the CAD model and establish global bounds. Finally, x_{tr} was constrained to a maximum of fraction of c_{tr} of the total length in Eq. (4).

$$\boldsymbol{x} = \{R_e, L, x_{tr}, d_1, d_2\}^T \tag{1}$$

$$\begin{aligned} R^* < R_e &\le R_{\max} \\ \varepsilon \le L_1 &\le L_{\max} \\ \varepsilon \le x_{tr} &\le L_{\max} \\ d_{\min} \le d_1, d_2 &\le d_{\max} \end{aligned} \tag{2}$$

$$\begin{aligned} R_e - R^* &\le L\tan(\beta_{\max}) \\ R_e - R^* &\ge L\tan(\beta_{\min}) \end{aligned} \tag{3}$$

$$x_{tr} \le c_{tr} L \tag{4}$$

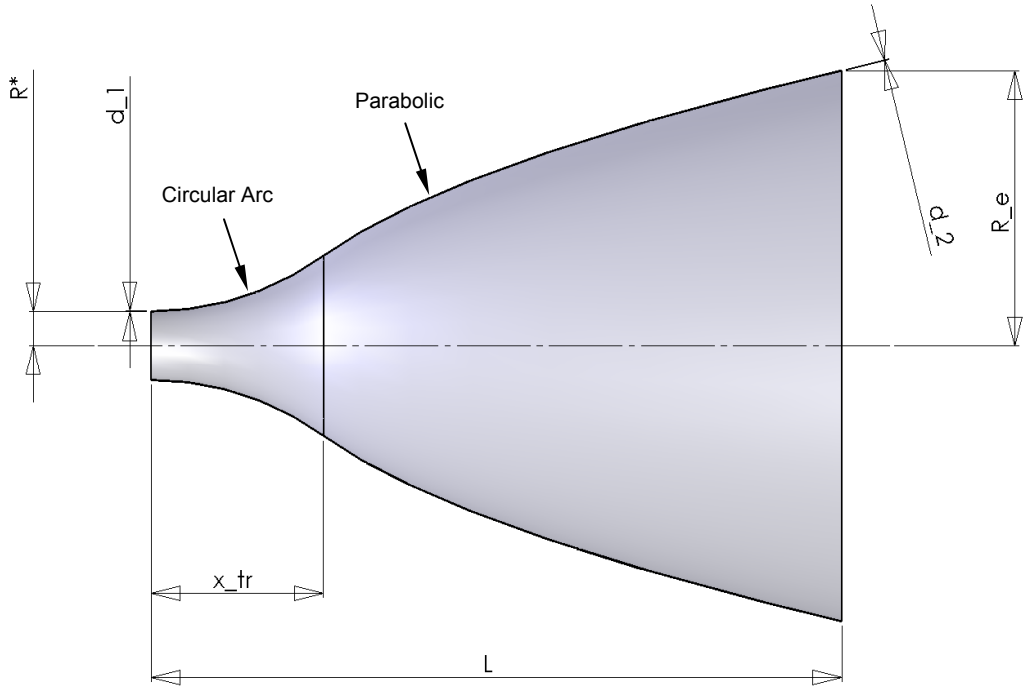

Figure 1. Side view of nozzle parametric profile.

Two different objective functions were used in order to test the MDO solution against the traditional design methods. In current practice, nozzles are generally designed for maximum thrust (C_F, Eq. (5)) or sometimes efficiency (I_{sp}, Eq. (6)). In this case the throat area and conditions are fixed, fixing the mass flow. Thus, the maximum C_F design and maximum I_{sp} designs are the same. After the propulsion system design is completed, the structure is analyzed and the material thicknesses set to meet the margin requirement. This practice will be followed for the first optimization, stated formally as a minimization problem in Eq. (7). The second will maximize the total stage velocity increment, ΔV, defined via the rocket equation in Eq. (8). Note that the design variables impact both I_{sp} and m_{nz} and that m_s has been explicitly separated from m_{nz}. Note that the exit area in Eq. (5) may or may not be normal to the nozzle axis and $\boldsymbol{x}$ is in this context is a unit normal vector in the axial direction (not to be confused with the design vector in Eq. (1) above).

$$C_F = \frac{F}{p^* A^*} = \frac{1}{p^* A^*} \int_{\text{exit}} (\rho(\boldsymbol{V} \cdot \boldsymbol{x}) + p(\boldsymbol{n}_e \cdot \boldsymbol{x}))dA \tag{5}$$

$$I_{sp} = \frac{C_F p^*}{\rho^* V^* g_0} \tag{6}$$

$$J_1 = -C_F \tag{7}$$

$$J_2 = -\Delta V = -I_{sp} g_0 \ln\left(\frac{m_P + m_S + m_{nz}}{m_S + m_{nz}}\right) \tag{8}$$

Finally, the static structural margin of safety (MS) must be constrained to a minimum value, MS_{min}, as stated in Eq. (9). It is possible, depending on the thrust level, temperature profile, and material thickness, that buckling near the throat may be important. Given the large internal pressure (which tends to resist buckling) such a situation is unlikely and neglected presently but is suggested by the author as a future direction. The evaluation of these objectives and constraints as well as the optimization architecture is discussed in detail in the subsequent sections.

$$c(\boldsymbol{x}) = MS_{min} - MS \leq 0 \tag{9}$$

III. Response Surface Approach

Global optimization problems which require computationally expensive physical data frequently utilize response surfaces to approximate the objective or constraint function(s), providing a continuous approximation of both the function value and gradient throughout the design space with a limited number of data samples. Here, we use the Kriging surface approach of Refs. (6,7,10,11) for physical data requiring an external computational tool (discussed individually in subsequent sections). Following the method of Ref. (6), the objective and constraint functions are adaptively sampled as needed based on the expected improvement function (EIF), increasing the fidelity of the solution near the eventual optimum. Since the EIF typically has numerous local maxima in regions between data, a genetic algorithm (GA) is well-suited to determine subsequent sample points. Here we use a standard GA algorithm for engineering applications discussed in Refs (3,4).

IV. Evaluation of Mass Properties and Geometry

The mass and derived geometry of the nozzle was evaluated through CAD application programming interface (API)[21]. In addition to the mass, various derived dimensions were recorded for later use in CFD meshing, discussed below. In this simple case, these values could be derived analytically but are accessed through the CAD interface in order to allow for future extensibility. Fig. 2 shows all the dimensions used (input and output) in addition to some superfluous dimensions used in sketching the original part. The mass, $m_{NZ}(\boldsymbol{x})$, and derived geometry data were used to create corresponding response surfaces as described in above.

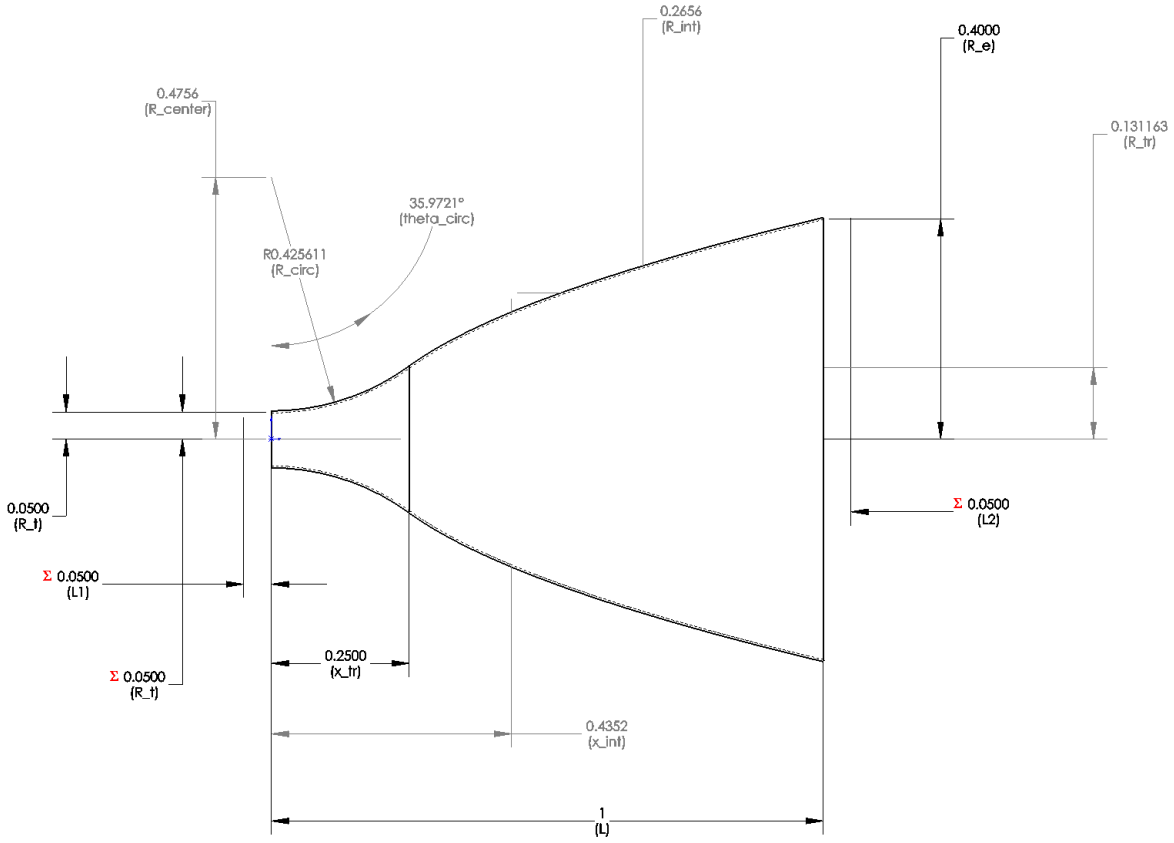

Figure 2. Nozzle profile with derived dimensions shown in grey. Dimensions preceded by a Σ symbol are bound via an equality constraint in the CAD model. Thicknesses d_1 and d_2 are not shown in this sectional view.

V. Evaluation of Propulsion Performance

The simulation of propulsion performance is discussed in this section. The combustion chamber properties, p_t and T_t, are additional scalar parameters and assumed constant for the purposes of this work. Between the chamber and throat, the Rayleigh relations of one-dimensional gasdynamics were used to estimate the loss in stagnation pressure

due to heat addition and, subsequently, the area-averaged throat conditions in Eq. (10). Note that the velocity in the chamber is taken as ≈ 0 and the throat has $M = 1.0$ by definition. A constant, average value of γ was used based on tabulated property data. T_t was assumed to be constant between the chamber and throat, though it is noted that heat transfer to the walls of the chamber and nozzle can be considerable. A higher-fidelity simulation of heat transfer is suggested by the author as a future direction.

$$\frac{p_t^*}{p_c} = \left(\frac{1+\gamma M_c^2}{1+\gamma M^{*2}}\right)\left(\frac{1+\frac{\gamma-1}{2}M^{*2}}{1+\frac{\gamma-1}{2}M_c^2}\right)^{\frac{\gamma}{\gamma-1}} \approx \left(\frac{1}{1+\gamma}\right)\left(1+\frac{\gamma-1}{2}\right)^{\frac{\gamma}{\gamma-1}} \tag{10}$$

The portion of the nozzle between the throat and exit was modeled with CFD. SUmb[23], a structured, multi-block, explicit Navier-Stokes solver developed at Stanford University, was used with a revolved, structured mesh. Automatic mesh generation is discussed in a subsequent section below. SUmb allows for the specification of temperature-dependent heat capacity, $c_p(T)$, as piecewise polynomials in T. These were generated from the equilibrium conditions of combustion products via the method discussed in the Appendix. The results, discussed below, were used to create response surfaces of $C_F(\boldsymbol{x})$ (for use in evaluating J) and $p_w(\boldsymbol{x},x)$ (for use in structural analysis).

A. Multi-Fidelity Approach

When computationally expensive analyses are used it is often of benefit to utilize multiple levels of fidelity to reduce the size of the design space and initialize subsequent analyses from a lower-fidelity solution. In the present work, the analysis of internal flow incurs the greatest computational expense and simple two-level approach is used. Euler (inviscid) CFD solutions are considerably less expensive than viscous solutions due to both a reduced mesh size and simplified physics. The optimization procedure is first performed with a propulsion performance response surface based on inviscid internal flow solutions. This procedure is then repeated with a propulsion performance response surface based on viscous internal flow solutions with an initial guess equal to the inviscid optimum.

In addition, the design space is reduced in size to surround the inviscid optimum to encompass a region with J within some fraction of J^*. Packing points more tightly around the inviscid optimum increases the accuracy of prediction locally but any reduction of the design space risks eliminating the global optimum when fidelity is tiered upward. Multi-fidelity response surface implementation is still an area of active research, and to the author's knowledge no general proof exists showing that a higher-fidelity MDO solution must exist within some quantifiable range of a lower-fidelity optimum. Intuitively, we expect the addition of viscous effects to have a small but significant impact on the optimum design but this is an acknowledged limitation of the simple "discrete" multi-fidelity method used here. In addition to the discrete jump in fidelity between viscous and inviscid analyses of the internal flow, continuous fidelity tuning is possible through CFD mesh resolution. Between these two, several tiers of fidelity could be used as desired or needed to reduce the cost.

B. Automatic Meshing for CFD Analysis

In order to generate a response surface based on CFD results, meshes of acceptable quality for any $\boldsymbol{x}$ in the feasible region of geometry need to be created in an automated fashion. The automatic meshing algorithm used here was developed to exploit axisymmetric geometry but could be extended with minimal modification to linear (rectangular) nozzles. A two-dimensional mesh was created between the centerline and the nozzle profile which was then revolved about the centerline to create a three-dimensional domain. For the sake of discussion, the topological mesh dimension along the profile from the throat to the exit plane is taken as the ξ–direction, the radial topological mesh dimension is taken as the η-direction, and around the nozzle (rotation to three-dimensions) as the θ-direction. In order to keep the aspect ratio of the three-dimensional cells ~$O(1)$, the number of cells in the ξ–direction was set such that the average spacing, Δs_ξ, was equal to a user-settable multiple, c_ξ, of the radial spacing, Δs_η, based on R_e. This is summarized in Eqs. (11-12). Values in the range $1.0 \le c_\xi \le 2.0$ were found to produce meshes of acceptable quality over a wide range of profiles. The ξ–direction spacing required the total arc length of the two sections, Eqs. (13–14), be summed. The spacing at the joint, Eq. (15), between the circular and parabolic sections was taken as the minimum of the two section spacings with the larger of the two reduced to match for a smooth transition. A hyperbolic tangent spacing law was used for all edges.

$$\Delta s_\eta = \frac{N_\eta}{R_e} \tag{11}$$

$$N_\xi = \frac{c_\xi}{\Delta s_\eta}\left(s_{circular} + s_{parabolic}\right) \tag{12}$$

$$s_{\xi_{circular}} = R_{circular}\Delta\theta_{circular} \tag{13}$$

$$s_{\xi_{parabolic}} = \frac{1}{2}(\sqrt{1+4A^2R_e^2} - \sqrt{1+4A^2R_{tr}^2}) + \frac{\sinh(2AR_e) - \sinh(2AR_{tr})}{4A}$$
$$A \equiv \frac{L - x_{tr}}{R_e^2 - R_{tr}^2} \tag{14}$$

$$\Delta s_{\xi_{joint}} = \min\{\Delta s_{\xi_{circular}}, \Delta s_{\xi_{parabolic}}\} \tag{15}$$

The number of divisions in each topological dimension was rounded to the nearest multiple of four for use with SUmb's three-level multigrid. Here, an elliptical smoothing method[13,15] was used to create the internal mesh. First the two-dimensional mesh was smoothed with to convergence. This mesh was revolved with eight divisions though 90° before the resulting three-dimensional mesh was again smoothed to convergence. Symmetry boundary conditions we applied to the $\theta_{\min}$ and $\theta_{\max}$ faces, an inviscid or viscous wall was used for the nozzle surface ($\eta_{\max}$) depending on the level of fidelity, an axisymmetric boundary was used at the axis of rotation ($\eta_{\min}$), a supersonic inflow was used at the throat ($\xi_{\min}$), and a supersonic outflow was used at the exit plane ($\xi_{\max}$). A typical inviscid mesh is shown in Fig. 3.

Viscous meshing required minimal adjustment to the automatic meshing algorithm. Rather than use a constant spacing Δs_η on the throat and exit planes a geometric spacing law was used with an initial normal spacing along the nozzle wall ($\xi_{\max}$) set to accommodate a turbulent boundary layer. The throat and exit plane viscous spacing values were set based on the core flow properties (estimated via one-dimensional gasdynamics) and the flat plate boundary layer correlation of Ref. (14) with a y^+ value of 1.0. This procedure results in cells with $\Delta s_\eta << \Delta s_\xi$ in the region near the nozzle wall. These cells can collapse or become inverted during smoothing for a number of reasons. Δs_η may be of the same order as the numerical tolerance and the enforcement of normal grid lines at the mesh corners are among them. While throat and exit planes perpendicular to the nozzle axis are preferred from simplicity in pre-processing and post-processing, they are not required. If mesh generation failed or a mesh quality check revealed cells of low quality, the exit plane was replaced with circular arc which was normal to both the axis and the end of the parabolic portion. This allowed normal mesh boundaries to be enforced on both the nozzle wall and exit surface simultaneously, often (but not always) improving mesh quality to acceptable levels. Very small angles between the parabolic portion of the profile and exit plane were found to result in meshes of the poorest quality.

Meshes were written in CGNS format[19] through Gridgen[20]. Parametrically created input files used Gridgen's Glyph scripting language for automated creation. Gridgen does not currently support all of the available CGNS boundary conditions, some of which were needed for these meshes (specifically, axisymmetry was needed along the axis). These boundaries were added after a given mesh was generated by directly accessing the CGNS file through the Fortran API.

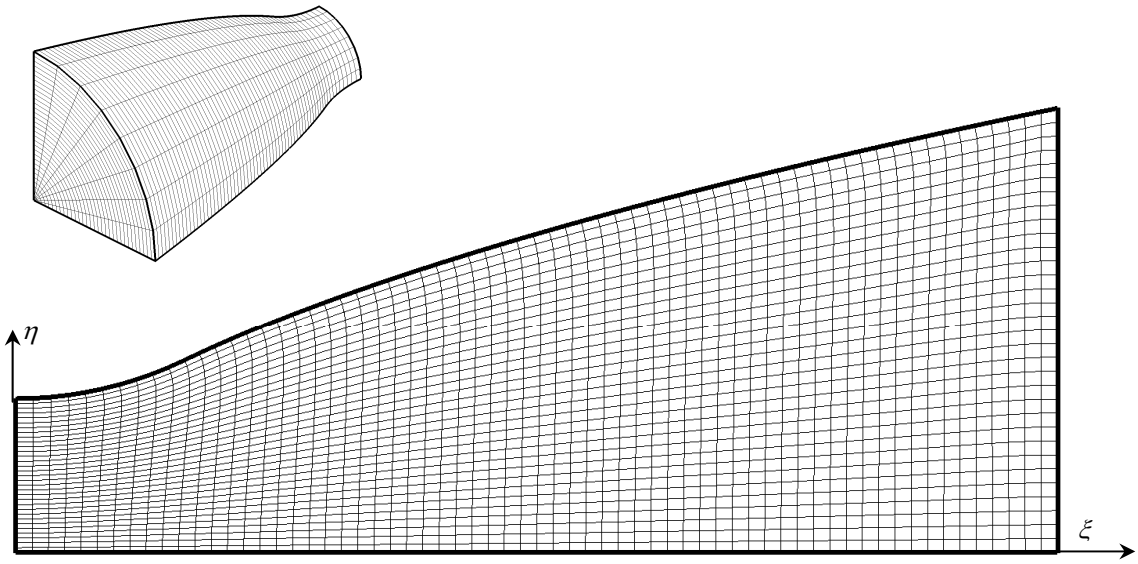

Figure 3. Side and isotropic views of an automatically-generated inviscid CFD mesh (64 x 32 x 8 cells = 16,384 total cells).

C. CFD Results & Response Surface Generation

Euler and Navier-Stokes CFD data were processed in the same way. The cell-centered data on the exit plane was extracted from the CGNS file before C_F and I_{sp} were computed by summing the discrete data in Eqs. (16-18). The area of each quadrilateral cell was computed with Eq. (18), where the subscripts 1-4 denote the coordinates of the corners. (The factor of four in Eq. (16) arises from the use of a 90° slice in the CFD model.) $C_F(\boldsymbol{x})$ was stored as a response surface with $I_{sp}(\boldsymbol{x})$ computed from C_F as needed to evaluate J_2. Since the skin thicknesses have a negligible effect on the internal flow, only R_e, L, and x_{tr} (collectively $\boldsymbol{x}_{CFD}$) were used for a three-dimensional response surface. The entire response surface creation loop is summarized in Fig. 4. Mach and pressure contours (non-dimensional) from a typical solution are shown in Figs. 5-6.

$$C_F = \frac{4}{p^* A^*} \sum_{exit} (\rho_{cell} V_{cell}^2 + p_{cell}) A_{cell} \tag{16}$$

$$I_{sp} = \frac{C_F p^*}{\rho^* V^* g_0} \tag{17}$$

$$A_{cell} = \frac{1}{2} \left| (\boldsymbol{r}_3 - \boldsymbol{r}_1) \times (\boldsymbol{r}_4 - \boldsymbol{r}_2) \right| \tag{18}$$

In addition to C_F, the pressure along the wall of the nozzle is required for subsequent structural analysis. This was stored as a response surface as well, adding the axial coordinate x as a continuous dimension to the abridged design vector $\boldsymbol{x}_{CFD}$, $p(\boldsymbol{x}_{CFD}, x)$.

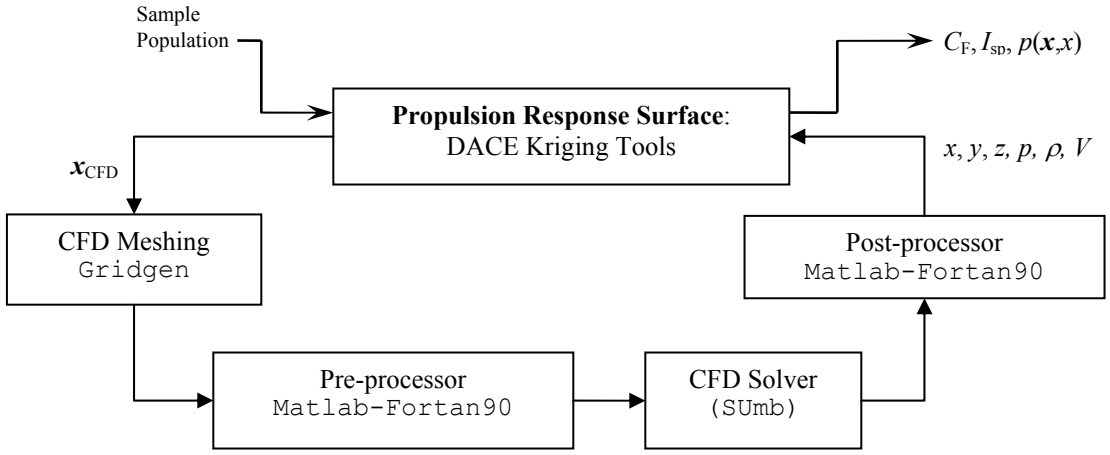

Figure 4. Summary of the response surface creation process for propulsion performance, including software tools.

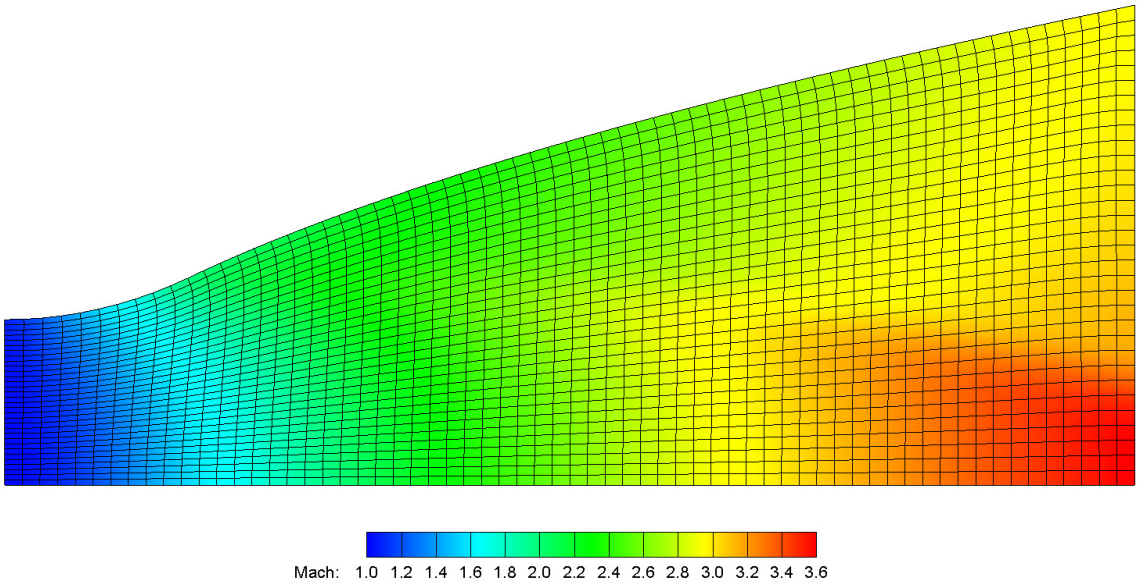

Figure 5. Mach contours of an inviscid solution with relatively low mesh resolution.

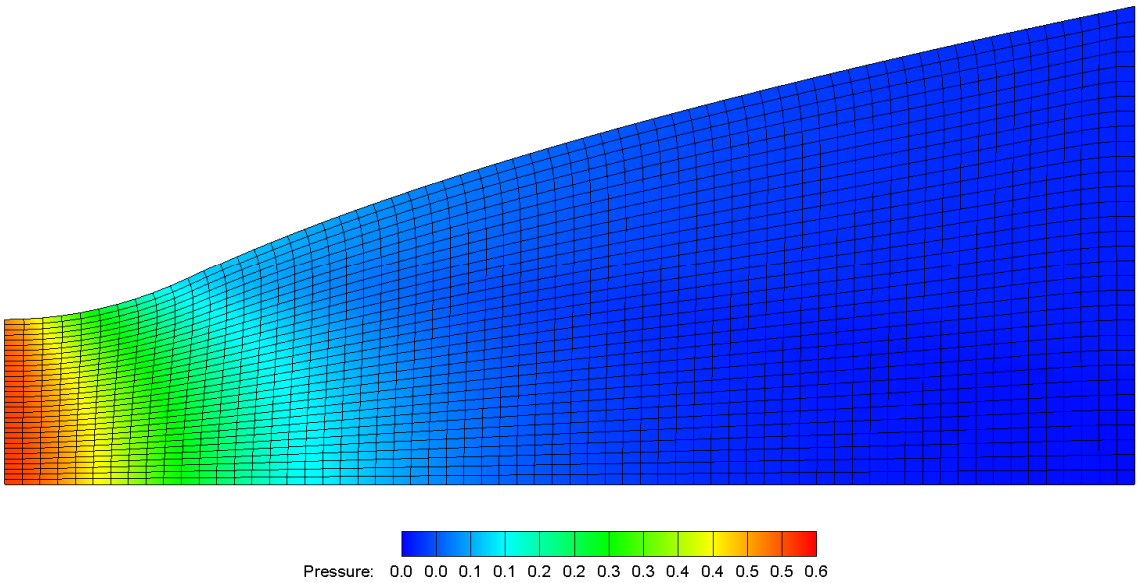

Figure 6. Pressure contours (p/p^*) of an inviscid solution with relatively low mesh resolution.

VI. Structural Analysis

Structural analysis was sufficiently simple in this case to be accurately treated analytically. It was assumed that all the structural loading came in the form of 1) membrane stresses in the hoop direction due to internal pressure and 2) compressive stresses in the axial direction to the thrust. Analytical treatment of the hoop stress via axisymmetric theory[17] is accurate provided the thin-walled assumption, $d << R$, is met. The axial (meridian) stress is determined by computing the portion of the thrust produced by the portion of the nozzle aft of a given point on the surface and dividing this by the local cross-sectional area. It should be noted that this neglects the stresses due to local bending in the membrane, which are presently neglected as relatively small. In order to capture these additional stress effects, a higher-fidelity analysis such as FEA would be needed and is suggested as a future direction. The characteristic radius R_2, defined in Ref. (17), is required for the analytical treatment. Assuming the profile $R(x)$ is available from the CAD data and basic geometry, R_2 is given by Eqs. (16–17). The stress in the meridian direction due to thrust is given by Eqs. (18–19).

$$\phi = \tan^{-1}\left(\frac{dR}{dx}\right) \tag{16}$$

$$R_2 = \frac{R}{\cos(\phi)} \tag{17}$$

$$F(x) = 2\pi \int_x^L p(y)R(y)\sin(\phi)dy \tag{18}$$

$$\sigma_m = -\frac{F}{2\pi R d\cos(\phi)} \tag{19}$$

Since Columbium is a ductile material, the von Mises stress is used as the yield criterion. This is compared with the material yield stress to compute the static margin in Eq. (20). A typical set of results is plotted in Fig. 7.

$$MS \equiv \frac{\sigma_{fail}}{\sigma} - 1 = \frac{\sigma_y}{\max\{\sigma_{VM}\}} - 1 \tag{20}$$

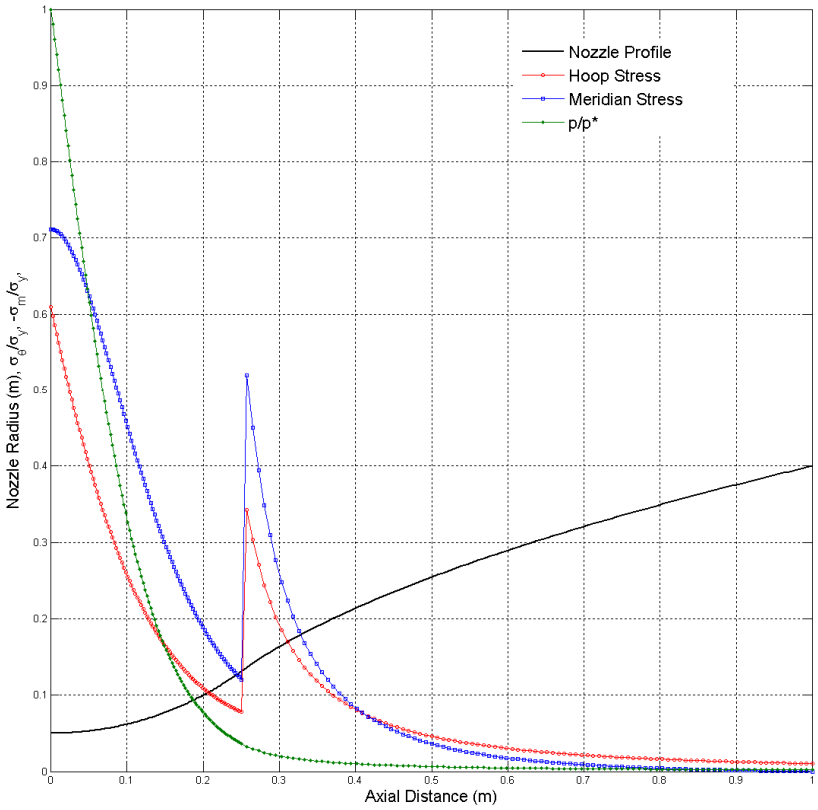

Figure 7. Stress profiles corresponding to the design in Fig. 1. d_1 = 0.5 mm and d_2 = 0.1 mm. Note that σ_m is actually negative in sign by convention for compressive stress ($-\sigma_m$ is shown). The discontinuity in stress at the circular-parabolic interface is due to the inflection point in R_2 and ϕ. In a real structure this would be a stress concentration smoothly varying over a short region.

VII. Optimization

By design, the procedure discussed in the sections above is independent of the optimizer chosen. Depending on the behavior of the objective and constraint functions' response surfaces, a gradient-based optimization algorithm or GA may perform better. If discrete variables are introduced, a GA is required. In the present work we use a SNOPT[2], implemented through TOMLAB[24]. This tool was found to perform well with this simple five-dimensional problem and more rigorous applications are suggested as a future direction below.

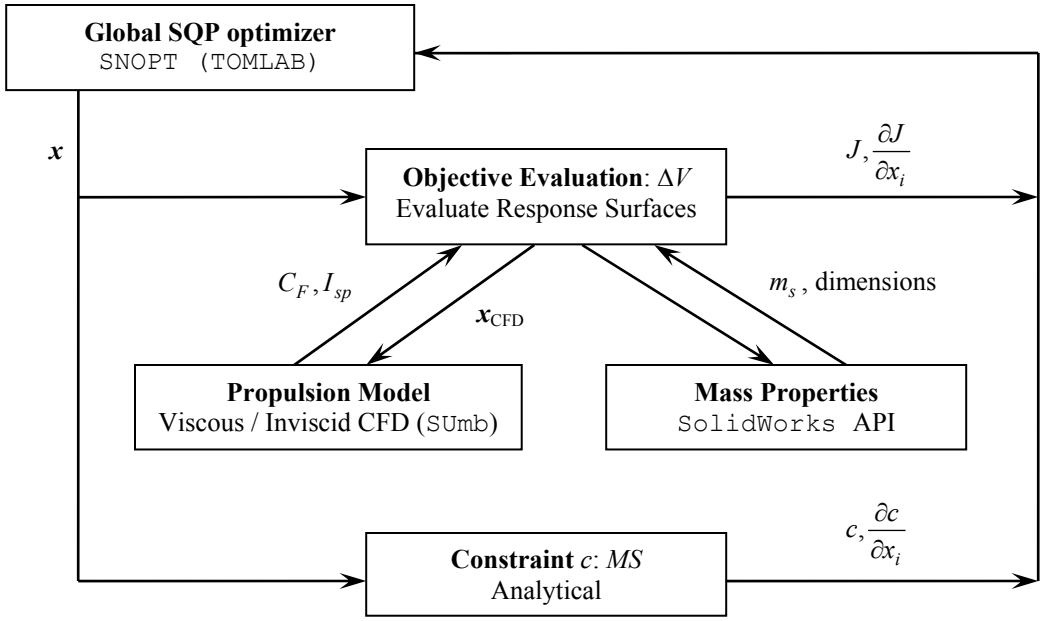

Figure 8. Information flow for a given design evaluation, including software tools. Configuration shown for MDO use; with C_F or I_{sp} as the objective the process is simplified to simply evaluating the propulsion performance response surface.

VIII. Example Problem

A liquid-oxygen (LOX) methane (CH_4) vacuum nozzle was chosen as a demonstration. This particular pair of propellants does not frequently find use in launch vehicles on Earth but has been suggested for in-situ propellant utilization on Mars[16]. The physical limits and parameters are summarized below (recall working units for $\boldsymbol{x}$ discussed above). Note that the chamber conditions are fairly arbitrary. The material chosen was Columbium, used in radiation-cooled nozzles due to its high melting temperature.

Dimension Limits:

$R^* = 5.0$ cm
1.0 cm $\le R \le$ 1.0 m
1.0 cm $\le L \le$ 2.0 m
0.4 mm $\le d \le$ 1.0 cm
$5° \le \beta \le 45°$
$c_{tr} = 0.90$

Vehicle Parameters:

m_S = 100 kg (not including m_{NZ})
m_P = 1,000 kg

Chamber and Throat Properties (based on a constant, average value of $\gamma = 1.14$):

p_c = 5.400 MPa
T_c = 3000 K
p^* = 2.523 MPa
T^* = 2804 K
ρ^* = 2.256 kg/m^3
V^* = 1,058 m/s

Material Properties:

ρ = 8,600 kg/m^3
E = 103 GPa
σ_y = 207 MPa
σ_{ult} = 300 MPa

Multi-Fidelity Settings:

Structural Analysis	= one level (low fidelity, thin-walled axisymmetric theory[17])
Mass Properties	= one level (high fidelity, computed via CAD API[21])
Internal Flow	= two levels (inviscid CFD, viscous CFD)
Fidelity Mapping (Internal Flow)	= level two bounded by $(J - J^*)/J^* = 0.10$, J^* from level one optimization

Optimization Settings:

Optimizer	= continuous, gradient-based (SQP)
Gradients	= automatic differentiation, implemented through Ref. (22)
Convergence Tolerance	= 10^{-6}
Feasibility Tolerance	= 10^{-6}

Response Surface Settings:

Dimensionality:	= 3 (CFD) or 5 (Mass Properties)
Initial Population Size:	= 61
Adaptive Sampling Population Size	= 20
Total Sample Population:	= 81
Correlation Function:	= Exponential
Regression Function:	= Second-order
Correlation Factor Range:	= $1.0 < \nu < 4.0$

Initial Feasible Design:

$\boldsymbol{x}_0$ = $\{0.4000, 1.0000, 0.2500, 1.000, 0.4000\}^T$
C_F = 3.1600
I_{sp} = 340.7 s
m_{NZ} = 2.343 kg
ΔV = 7,944 m/s
MS_{min} = 0.7460

The optimum solutions are summarized below. For each solution, the relevant propulsive performance data is shown in addition to the mass and structural margin of the nozzle. In comparing the final objective, ΔV, we find that the traditional methodology results in only a 0.44% improvement despite relatively large improvement in C_F and I_{sp} (+7.72%). This is due to the corresponding increase in the mass of the much larger optimum-thrust nozzle. When considering the multidisciplinary optimum, including the contributions of mass and structural margins to performance, a 1.51% improvement is made in ΔV; a factor of 3.4 larger than the gain of the traditional design. For the basis of comparison, it is important to note that no diverging nozzle (only a choked, converging nozzle) would produce an ideal $C_F = \gamma + 1 \approx 2.14$, $I_{sp} \approx 213.4$ s, and a corresponding $\Delta V \approx 4{,}820$ m/s (based on one-dimensional flow with area-averaged properties). When analyzing nozzle performance, seemingly small improvements are quite significant.

A. Traditional Optimum (J_1)

Recalling the tradition design methodology from above, C_F was maximized over the feasible region and the material thicknesses subsequently solved for much that $MS > 0.10$ throughout. The resulting design is shown in Fig. 9. Note that this design is considerably larger in size than the initial feasible design (Fig. 2) and the length is

maximized, but not the radius. This means the highest C_F design does not correspond to the highest area ratio, which one-dimensional compressible flow would predict. This emphasizes the importance of three-dimensional flow losses to overall performance.

Optimum Design:

$\boldsymbol{x}^* = \{0.6353, 2.500, 0.2853, 0.6642, 0.4000\}^T$
$C_F = 3.4038$
$I_{sp} = 367.0$ s
$m_{NZ} = 22.37$ kg
$\Delta V = 7{,}979$ m/s
$MS_{min} = 0.1000$

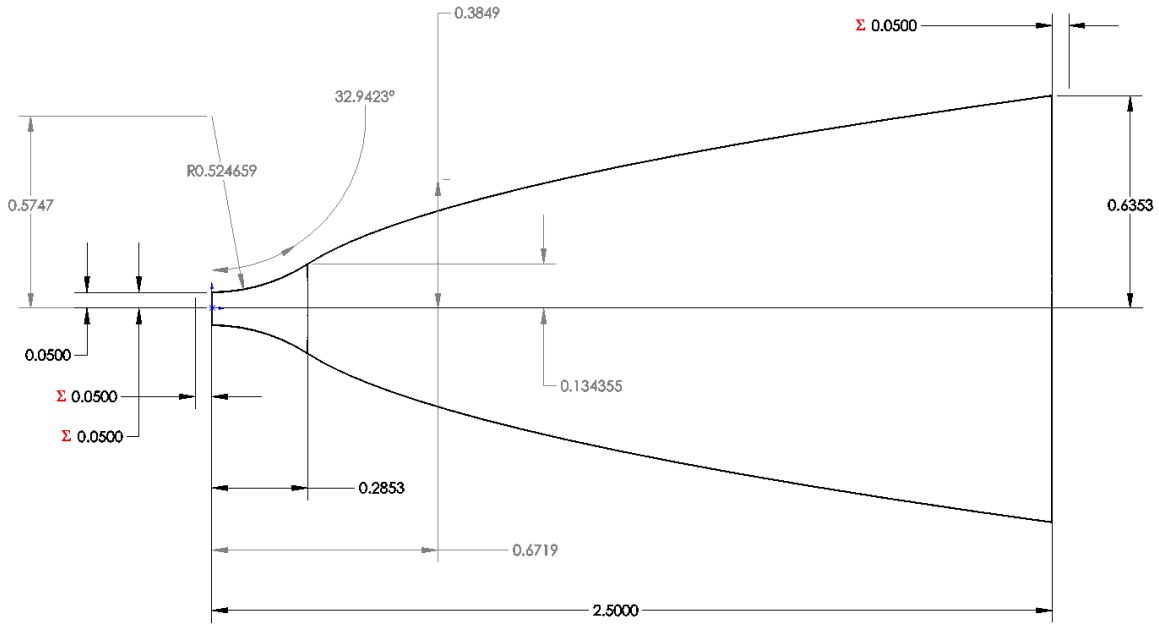

Figure 9. Optimum design based on the traditional method maximizing C_F and adjusting thicknesses to meet the structural requirement.

B. Multidisciplinary Optimum (J_2)

The MDO solution, shown below in Fig. 10, is significantly different than the traditional optimum. Notably, neither the length nor exit radius is maximized and the circular arc section is minimized. Qualitatively, this solution represents a compromise between mass and propulsive performance. At the size determined by the optimization, the profile very closely resembles that of traditional characteristic-based nozzle optimum designs ("bell" shaped nozzles)[1,8,9,18]. Similar to the optimum above, the MDO solution has minimized the skin thicknesses such that the minimum MS is exactly met as expected.

Even in an example this simple (containing only three analytical disciplines), the benefits of a multidisciplinary approach can be seen. Given that the nozzle design, within global bounds and at fixed throat conditions, can only have a small effect on the overall stage performance the relative gains associated with the MDO and traditional solutions are considerable.

Optimum Design:

$\boldsymbol{x}^* = \{0.4078, 1.514, 0.0100, 0.8471, 0.4000\}^T$
$C_F = 3.2889$
$I_{sp} = 354.6$ s

$m_{NZ} = 9.218$ kg
$\Delta V = 8{,}064$ m/s
$MS_{min} = 0.1000$

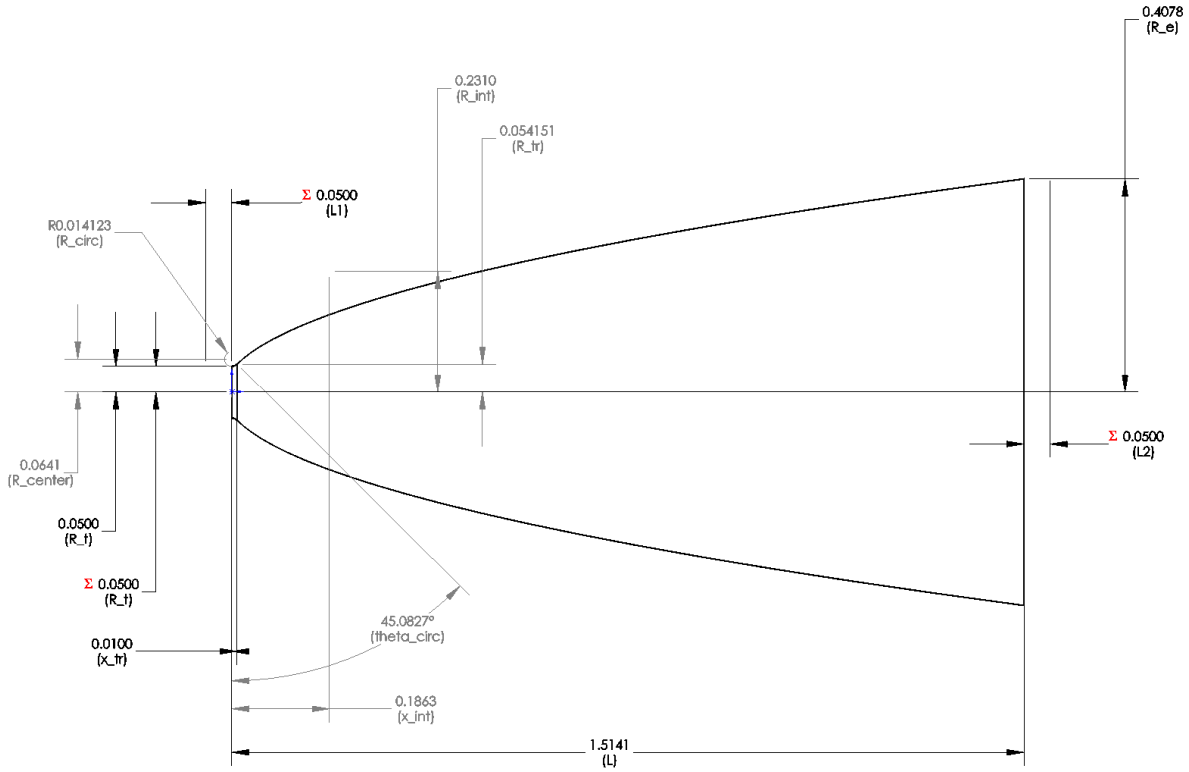

Figure 10. Profile of multidisciplinary optimum design. Note that this nozzle is considerably smaller that the corresponding traditional optimum shown in Fig. 9, above.

IX. Conclusions & Future Work

In this work an optimizer-independent MDO framework for the optimization of vacuum nozzles was developed and compared to traditional methodologies. In constructing the analytical framework, a combination of readily-available commercial and university-based software tools was used with a focus on flexibility, scalability, and extensibility. A relatively simple nozzle profile was tested for the purposes of demonstration, revealing the benefits of an MDO-based approach to nozzle design.

There are many opportunities to extend this research to more advanced and higher-fidelity applications. Generalizing the nozzle architecture to a spline with discrete control points would allow foe a much broader range of solutions while increasing the problem dimensionality considerably. Increased problem dimensionality results in more expensive response surface generation and evaluation in addition to increasing the cost of the optimization procedure. These challenges, however, do not modify the current framework. The greatest difficulty in generalizing the profile is automatic meshing for CFD analyses. If a structured mesh and solver are to be retained, the procedure discussed above would require generalization. Alternatively, an unstructured approach is possible but a viscous boundary layer region would still be required if viscous CFD were retained.

In addition to generalizing the geometry, adding higher-fidelity physics to the MDO process would increase the value of this framework as a practical design tool. The greatest omission in the current procedure is some accounting of heat transfer in the nozzle wall. For a vacuum nozzle which is radiatively cooled, a straightforward approach could be used to determine the equilibrium heat transfer but the difficult lies in: 1) integrating these results into the flow solution and 2) establishing a constraint or objective function which includes the effects of heat transfer on performance. These difficulties are reflective of a more general difficulty with MDO: communicating data through interdependent analyses. Accounting for heat transfer in the walls changes both the material properties for subsequent structural analysis and the internal flow solution used to evaluate propulsive performance. It would also be of benefit to include regenerative nozzle designs in which heat transfer plays a more central role.

Two other area in which fidelity could be increased are structural analysis and the thermochemistry of the internal flow. Moving to a finite element analysis (FEA) of the nozzle would provide more accurate results and allow for more advanced materials to be considered but also increase the computational cost dramatically (compared to the simple analytical expressions used here). In addition structural stability (buckling), presently neglected, could be included. It is worth noting that this would require additional response surfaces to be formed and evaluated. Internal flow in the high-temperature region of the nozzle can be significantly affected by the local thermochemistry and a coupled thermodynamic-flow solutions would improve the accuracy of prediction. Here, we have accounted for variations in the specific heats with T but assumed that $\Re$ and Pr are constants with the ideal gas equation of state. Improving fidelity in this case requires integrating thermochemical equilibrium into a CFD solver – an extensive undertaking.

Finally, this procedure would benefit as a practical design tool via the inclusion of more specific manufacturing and material constraints, even adding material selection as a discrete variable. With discrete variables included (e.g. material thicknesses), a GA must be used over a SQP or similar gradient-based method. While this does not alter the architecture discussed here, a much more expensive optimization process can result. In engineering optimization applications GAs are powerful but often suffer from slow convergence rates when compared to SQP algorithms such as SNOPT. In addition, mixed sets of continuous and discrete variables increase the difficulty of using Kriging surfaces in the manner discussed above which are developed on continuous variables.

Appendix

In order to accurately simulate the internal flow in the nozzle, the properties of CH_4-O_2 combustion products were investigated in the range of pressures and temperature typical of chemical engines. Though the flow is chemically reaction throughout the entire nozzle flow, the majority of the total thermal energy is released between in the combustion chamber and between the chamber and the nozzle throat. Between the throat and exit planes, the combustion products can be treated accurately as a mixture of fixed chemical composition but varying thermodynamic properties. Specifically, the ratio of $c_p/\mathcal{R}$ was specified as a polynomial assuming a constant molecular weight.

To determine $c_p/\mathcal{R}$ as a function of T, STANJAN[22] was used to calculate the equilibrium properties and chemical composition of CH_4-O_2 combustion products using a nominal O/F ratio of 3.20 by mass[12]. Since the equilibrium properties are primarily a function of T, an isentropic expansion was used to match p to T through the nozzle. The resulting polynomial dependence of $c_p/\mathcal{R}$ is shown in (6).

$$900\text{ K} - 2000\text{ K} \qquad \frac{c_p}{\Re} \approx (2.097x10^{-13}K^{-4})T^4 - (1.316x10^{-9}K^{-3})T^3 + (3.753x10^{-6}K^{-2})T^2 - (4.996x10^{-3}K^{-1})T + 8.088 \tag{21}$$

$$2000\text{ K} - 3100\text{ K} \qquad \frac{c_p}{\Re} \approx (9.278x10^{-13}K^{-4})T^4 - (1.197x10^{-8}K^{-3})T^3 + (5.537x10^{-5}K^{-2})T^2 - (1.079x10^{-1}K^{-1})T + 8.109 \tag{22}$$

It should be noted that the molecular weight does, in fact, change slightly between T^* and 900 K. The resulting variation in $\mathcal{R}$ is absorbed into the ratio $c_p/\mathcal{R}$.

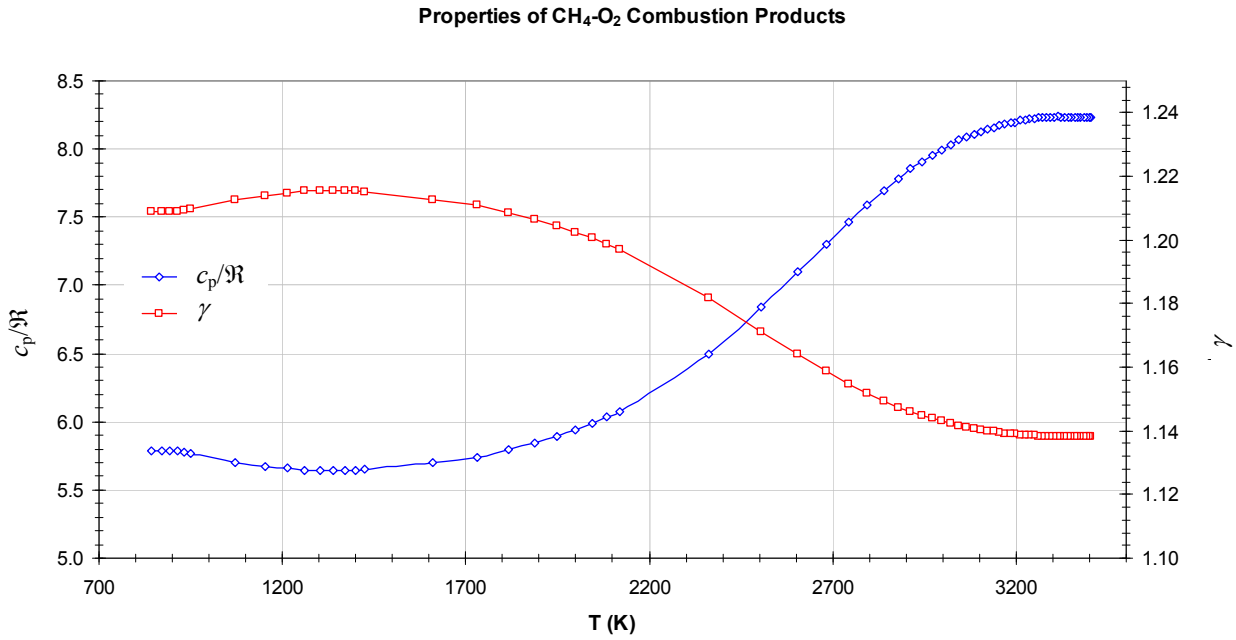

Figure 11. Numerically calculated equilibrium values of the ratio of specific heats, γ, and $c_p/\Re$ vs. T.

Acknowledgments

The author would like to thank Wenny Wang of Pointwise, Inc. for her help in implementing the automatic meshing algorithm in Gridgen.

References

[1]Farley, J. M. and Campbell, C. E., "Performance of Several Method of Characteristics Exhaust Nozzles", NASA TN-D293, Oct. 1960.

[2]Gill, P. E., Murray, W., and Saunders, M. A.,"SNOPT: An SQP Algorithm for Large-Scale Constrained Optimization," *SIAM Review*, Vol. 47, No. 1, 2005, pp. 99-131.

[3]Holst, T. L. and Pulliam, T.H., "Evaluation of Genetic Algorithm Concepts Using Model Problems, Part I: Single Objective Optimization", NASA/TM-2003-212812, 2003.

[4]Holst, T. L. and Pulliam, T.H., "Evaluation of Genetic Algorithm Concepts Using Model Problems, Part II: Multi-Objective Optimization", NASA/TM-2003-212813, 2003.

[5]Huzel, D. K., and Huang, D. H., *Modern Engineering for Design of Liquid Rocket Engines*, AIAA, 1992.

[6]Jones, D. R., Schonlau, M., and Welch, W.J., "Efficient Global Optimization of Expensive Black-Box Functions", *Journal of Global Optimization*, Vol. 13, No. 4, Dec. 1998, pp. 455-492.

[7]Lophaven, S. N., Nielsen, H. B., and Søndergaard, J., "DACE: A Matlab Kriging Toolbox", Technical Report *IMM-TR-2002-12*, Technical University of Denmark, Version 2.0, 2002.

[8]Rao, G. V. R., "Exhaust Nozzle Contour for Optimum Thrust", *Jet Propulsion*, Vol. 28, No. 6, June 1958, pp. 377-382.

[9]Rao, G. V. R., "Recent Developments in Rocket Nozzle Configurations", *ARS Journal*, Vol. 31, No. 11, Nov. 1961, pp. 1488-1494.

[10]Simpson, T. W., Mauery, T. M., Korte, J. J., and Mistree, F., "Kriging Models for Global Approximation in Simulation-Based Multidisciplinary Design Optimization", *AIAA Journal*, Vol. 39, No. 12, Dec. 2001, pp. 2233-2241.

[11]Sóbester, A., Leary, S.J., and Keane, A. J., "On the Design of Optimization Strategies Based on Global Response Surface Approximate Models", *Journal of Global Optimization*, Vol. 13, Sept. 2005, pp. 31-59.

[12]Sutton, G. P. and Biblarz, O., *Rocket Propulsion Elements,* 7th Edition, John Wiley & Sons, 2001, Chap. 5-9.

[13]Thomas, P. D. and Middlecoff, J. F. "Direct Control of the Grid Point Distribution in Meshes Generated by Elliptic Equations", *AIAA 79-1462R*, Vol. 18, No. 6, 1980, pp. 652-656.

[14]White, F. M., *Viscous Fluid Flow,* 2nd Edition, McGraw Hill, 1991, Chap 7.

[15]White, J. A., "Elliptic Grid Generation With Orthogonality and Spacing Control on an Arbitrary Number of Boundaries", *AIAA 90-1568*, June 1990.

[16]Zubrin, R. M., Baker, D. A., and Gwynne, O., "Mars Direct: A Simple, Robust, Cost Effective Architecture for the Space Exploration Initiative", *AIAA-91-0328*, Jan. 1991.

[17]"Astronautical Structures Manual, Vol. 2", NASA TM X-7330, Aug. 1975.

[18]"Liquid Rocket Engine Nozzles", NASA SP-8120, July 1976.

[19]CGNS (CFD General Notation System), Software Package (open source), Ver. 2.4.2, www.cgns.org, 2007.

[20]Gridgen, Software Package, Ver. 15.09, Pointwise, Inc., 2007.

[21]SolidWorks Office Professional API, Software Package, Ver. 2006 SP 5.1, Dassault Systems, 2006.

[22]STANJAN, Software Package, Ver. 3.89, Stanford University Mechanical Engineering (Prof. W. C. Reynolds), 1987.

[23]SUmb, Software Package, Stanford University Aeronautics & Astronautics, 2007.

[24]TOMLAB, Software Package, Ver. 5.9, Tomlab Optimization, 2007.